ARCHIVES OF ELECTRICAL ENGINEERING VOL. 66(4), pp. 843-854 (2017)

DOI 10.1515/aee-2017-0064

A new circuit topology using Z-source resonant inverter for high power contactless power transfer applications

PRABHAT CHANDRA GHOSH[1], PRADIP KUMAR SADHU[1], ANKITA GHOSH[2], NITAI PAL[1]

[1]*Department of Electrical Engineering*
Indian Institute of Technology (ISM), Dhanbad-826004, India

[2]*Department of Electrical Engineering*
PVG's College of Engineering and Technology, Pune-411003, India
e-mail: pcghoshcme@gmail.com

(Received: 24.04.2017, revised: 15.09.2017)

Abstract: In this study, a new circuit topology using a Z-source resonant inverter (ZSRI) for high power applications in large-air-gap contactless power transfer (CPT) systems, has been investigated. The main shortcoming of a large-air-gap CPT system is the poor power transfer efficiency due to low magnetic coupling. In order to minimize this shortcoming and to improve the overall performance of the system by boosting the power transfer capability, in this paper a CPT system with the newly developed circuit topology using high frequency Z-source resonant inverter has been proposed. Using the newly developed circuit topology for the CPT system, it has been observed that the overall performance of the system has been improved to a reasonable level with a purely sinusoidal resonant current flowing through the primary side. Therefore, no harmonics will be injected into the source. The proposed CPT system with an air gap of 16 cm and a misalignment of 3 cm has been simulated using the Maxwell finite element tool and Simplorer circuit simulation software for an output power of 2 kW.

Key words: contactless power transfer, mutual inductance, magnetic coupling coefficient, Z-source, resonant inverter

1. Introduction

Contactless power transfer (CPT) systems are designed to transfer power efficiently from a stationary primary coil to a stationary or movable secondary coil through an air gap. Contactless means inductive coupling between two objects through an air gap [1-3]. The fundamental principle of a CPT system is similar to the closely coupled electrical and electromechanical devices such as transformers and induction motors in which leakage inductance is

very low due to high magnetic coupling. But CPT systems are operated at a large air gap resulting in high leakage inductances and low magnetic coupling. Due to high leakages and low magnetic coupling, CPT systems have very poor power transfer efficiency [4-6]. In order to offset the effect of low magnetic coupling due to high magnetic leakages, CPT systems are generally operated at high frequencies to improve the quality factor of the CPT transformer. On the other hand, at high frequencies, losses in the system will be increased due to high switching losses of the inverter and thereby affecting the overall power transfer efficiency of the system. To overcome this drawback, CPT systems are commonly operated at resonant frequency by incorporating compensating capacitors [7-9]. Presently, the operational frequency for high power CPT systems is below 100 kHz due to high switching losses at a high frequency. Additionally, resonant circuits reduce the reactive power requirement for the system thereby boosting the overall power transfer capability and minimizing the VA (volt-ampere) ratings of the system [10-12].

Recently, rapid advancement in power electronics has enabled many new applications of CPT systems like contactless battery charging for electric vehicles, compact electronic devices, mobile phones and medical implants [13-15]. CPT systems are also very useful for power supplies in harsh environments such as mining, outdoor lightings, etc. The main advantages of contactless power transfer are safety, reliability, low maintenance and long product life [16]. While comparing to power transfer through conventional transformer, CPT technology is having more complex systems. Because of the increasing areas of applications of this technology, a lot of new solutions with very different technical requirements (e.g. voltage and power level, transfer distance, installation size) are necessary. To allow an efficient and safe power transfer, the entire CPT system should be carefully designed for a particular application. Therefore, new concepts of designs for both, magnetic and power electronic devices, are desirable. Usually, the design development is carried out by extensive experimental analysis and iterative practical redesigns. Resonant inverters play important roles in CPT systems. However, voltage source resonant inverters commonly used in CPT systems are having some inherent drawbacks. In this paper, to overcome the drawbacks of the conventional voltage source resonant inverters, a newly developed Z-source resonant inverter (ZSRI) with a Z-source network (ZSN) for high power contactless power transfer applications has been proposed.

The ZSN in the proposed ZSRI provides the unique feature of inherent power factor correction (PFC) without adding extra switching devices. It is possible because it adds the unique features of immunity to the H-bridge inverter during shoot-through states. This characteristic makes the input current as a sinusoidal waveform and in phase with the *ac* input voltage. This variable also provides a boost factor to the system. Therefore, it is normally used for voltage regulation [17, 18]. However, to regulate the output voltage, the proposed ZSN-based inverter uses the active state duty cycle, which is a common control variable used in series resonant inverters. Both control variables are used in the series resonant H-bridge inverter and the ZSRI does not require additional control circuitry to provide power factor correction. In other words, because of the ZSN, the ZSRI can perform power factor correction as well as *dc*/*ac* conversion in single stage. In the next section, modelling and detailed analysis of the proposed circuit has been discussed.

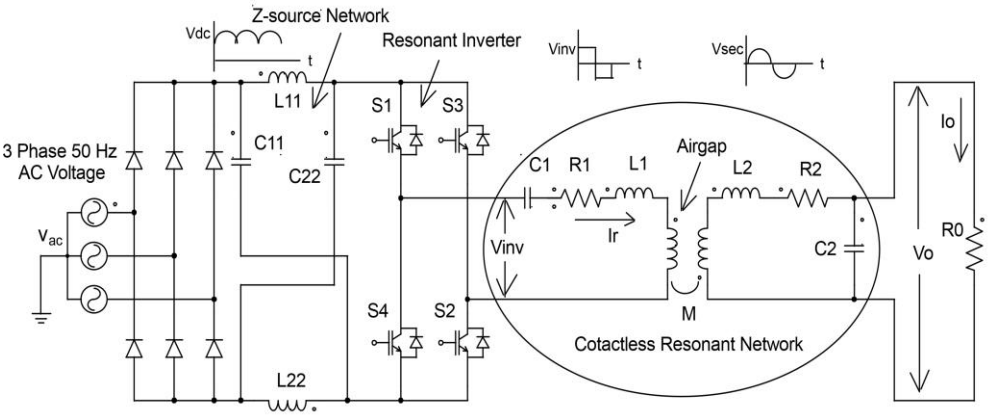

Fig. 1. Equivalent circuit model of the proposed CPT system

2. Analysis and modelling of the proposed CPT system

Fig. 1 shows the main circuit configuration of the proposed CPT system with a Z-source resonant inverter (ZSRI). The Z-source network consisting of inductors L_{11}, L_{22} and capacitors C_{11}, C_{22} is connected to the rectified *dc* output of a three phase *ac* voltage source. In the present circuit, at first three phase *ac* voltage v_{ac} (phase voltage) is rectified into *dc* voltage V_{DC} by a diode bridge rectifier. This *dc* link voltage serves as the *dc* input voltage to the Z-source network. The *dc* output voltage V_i of the Z-source network is converted into a high frequency single phase *ac* voltage by an IGBTs-based full-bridge resonant inverter for CPT system. In the present CPT system, series-parallel (SP) compensation topology has been used [19-23]. Analysis of the Z-source network along with the CPT system has been described below.

2.1. Operation during active state or non-boost mode

For the analysis of the Z-source network for the CPT system, the *ac* voltage source along with the diode bridge rectifier has been replaced with a *dc* voltage source with absolute value of $|v_{ac}|$ of *ac* input voltage v_{ac} in series with switch S_1 as shown in Fig. 2. The full-bridge resonant inverter is replaced with a single switch S_2. The resonant circuit, contactless transformer and the load have been replaced by a single sinusoidal current source i_r, since at resonance a sinusoidal current is always flowing through the resonant circuit at any instant as shown in Fig. 2. Assuming the Z-source capacitors and inductors are equal, $C_{11} = C_{22} = C$, $L_{11} = L_{22} = L$ and voltages $v_{C11} = v_{C22} = v_C$ and $v_{L11} = v_{L22} = v_L$. In the active state, two diagonal switches in the inverter are ON while the other two switches are OFF. Total time interval of two active states is T_A in one switching period T_{SW}. So, during each active state, the time interval is $T_A/2$ during one switching period.

During the active states, switch S_1 is ON and switch S_2 is OFF as shown in Fig. 3 [19-24]. During this state, capacitors are charged from rectified *dc* voltage and inductors. The *dc* vol-

tage across the inverter bridge is boosted and the power flows from the Z-source network and inverter to the resonant contactless power transformer and then to the load. From Fig. 3, the voltage v_L across inductors can be expressed as follows:

$$2v_L = |v_{ac}| - V_i = |V_m \sin \varpi t| - V_i = V_{DC} - V_i,\ v_C = 0. \tag{1}$$

where: v_{ac} is the *ac* input voltage (phase voltage), $|v_{ac}|$ is the absolute value of *ac* input voltage, V_m is the peak value of input *ac* voltage, V_{DC} is the *dc* input voltage to the Z-source circuit, V_i is the input voltage to the inverter.

From (1) we get

$$v_L = \frac{1}{2}(V_{DC} - V_i). \tag{2}$$

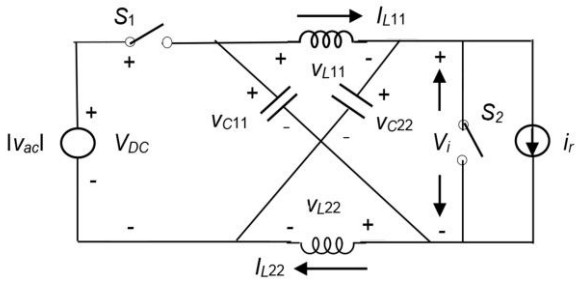

Fig. 2. Simplified equivalent circuit diagram of the Z-source resonant inverter with CPT system

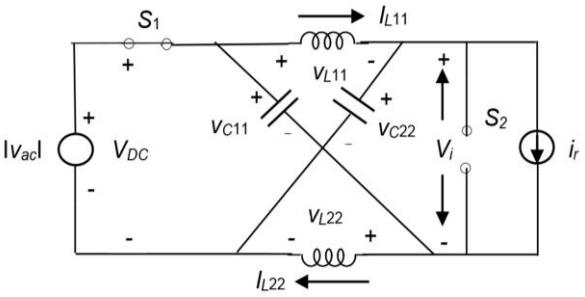

Fig. 3. Equivalent circuit diagram during active state

2.2. Operation during shoot-through state or boost mode

In this mode, three switches in the inverter bridge are ON and the remaining one can be either ON or OFF during the time interval of $T_S/4$ (T_S being the total shoot-through time interval in one switching period T_{SW}). During this mode, switch S_1 is OFF and switch S_2 is ON as shown in Fig. 4. The power is transferred from the capacitors to the inductors and consequently the *dc* link voltage across the input of the inverter is boosted [19-24]. The inductor voltage during the time interval of $T_S/4$ becomes equal to the capacitor voltage and is given by:

$$v_L = v_C . \tag{3}$$

During this boost mode, the conventional zero state is converted to shoot-through zero state. In this way, the sinusoidal output current is maintained and the voltage boost is achieved from the shoot-through of the *dc* link. The total time interval of four conventional zero states is T_0 ($T_0 = T_{SW} - T_A - T_S$). During the interval of $T_0/4$, two horizontal switches in the inverter bridge are ON, while the other two switches are OFF. Rectified *dc* voltage of the diode bridge rectifier and the inductors charge the capacitors, but no power flows to the resonant network. The inductor voltage during this time interval can be expressed as follows:

$$v_L = V_{DC} - v_C = \left|V_m \sin \varpi t\right| - v_C , \tag{4}$$

where: V_m is the maximum value of the input *ac* voltage v_{ac} (phase voltage), ω is the angular frequency.

Under steady state condition, the average of inductor voltage $\bar{V}_L$ becomes zero over one switching period of T_{SW}, the average voltage $\bar{V}_L$ can be expressed as follows:

$$\bar{V}_L = \frac{T_A}{T_{SW}}\left(\frac{\left|v_{ac}\right| - V_i}{2}\right) + \frac{T_S}{T_{SW}} v_C + \frac{T_0}{T_{SW}}\left(\left|v_{ac}\right| - v_C\right) = 0 , \tag{5}$$

where: $|v_{ac}|$ is the absolute value of *ac* input voltage v_{ac} (phase voltage) and switching periods, T_A, T_S, and T_0 are the active state, shoot-through state and conventional zero state time intervals respectively, T_{SW} is the total switching period. $T_{SW} = T_A + T_S + T_0$.

Now, the capacitor voltage of the Z-source network [17, 18, 25] can be expressed as:

$$v_C = \frac{1 - D_S}{1 - 2D_S}\left|v_{ac}\right| , \tag{6}$$

where the shoot-through state duty cycle

$$D_S = \frac{T_S}{T_{SW}} .$$

In the same way, the active state duty cycle $D_A = \dfrac{T_A}{T_{SW}}$.

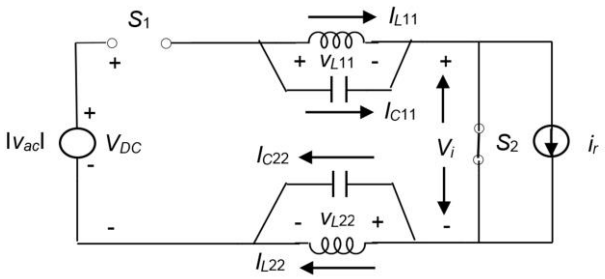

Fig. 4. Equivalent circuit diagram during shoot-through state

From (5) and (6), the shoot-through duty cycle can be expressed as:

$$D_S = \frac{V_i - |v_{ac}|}{2V_i}, \tag{7}$$

and

$$V_i = \frac{|v_{ac}|}{1-2D_S}, \tag{8}$$

where: V_i is the input voltage to the resonant inverter.

Assuming the system in continuous conduction mode, the average power across the resonant circuit can be derived as follows [19-22]:

$$\overline{P}_R(t) = \frac{1}{T_{SW}} \int_0^{T_{SW}} v_{inv}(t) i_r(t) \mathrm{d}t, \tag{9}$$

where $\overline{P}_R$ is the average power across the resonant circuit, v_{inv} is the output voltage of the resonant inverter and i_r is the resonant current flowing through the system.

The average output voltage and power can be expressed as:

$$\overline{V}_0(v_{ac}, D_A, D_S) = \frac{1}{T} \int_0^T v_o(t) \mathrm{d}t, \tag{10}$$

and

$$\overline{P}_o(v_{ac}, D_A, D_S) = \frac{1}{T} \int_0^T \overline{P}_R(t) \mathrm{d}t, \tag{11}$$

where: T is the time period of the input *ac* voltage (v_{ac}) and its value is 1/50 s, v_o is the *ac* output voltage across load resistance R_0, $\overline{V}_0$ is the average output voltage, $\overline{P}_o$ is the average output power.

From (10) and (11), it is clear that the output voltage and the output power can be regulated by controlling the *ac* input voltage, active state duty cycle and shoot-through duty cycle.

3. Simulation results and discussions

Simulation has been performed for the proposed system for high power applications using finite element tool (Maxwell) and circuit simulation software (Simplorer). Simulation parameters are given in Table 1. At first, finite element analysis (FEA) of the CPT transformer has been carried out for an air gap of 16 cm and misalignment of 3 cm as shown in Fig. 5.

Flux density distribution has been given in Fig. 6. The finite element analysis of the CPT transformer has also been performed for the relationship between the coupling coefficient and lateral misalignment for an air gap of 16 cm. Results have been shown in Fig. 7. It is observed from Fig. 7 that the maximum coupling coefficient can be achieved when the centre of the transmitter coil is aligned with the centre of the receiver coil and therefore maximum efficiency of the system is achieved at this position.

Using circuit simulation software (Simplorer), circuit simulation of the proposed CPT system as shown in Fig. 8, has been carried out by linking the FEM modules with the electrical circuit modules to compute the electrical transfer characteristics. The ZSRI design is based on [26] and [27]. The compensation capacitors were selected in such a way that the resonant frequency equals the switching frequency. Switching frequencies for such systems vary between 10 and 50 kHz [27-30]. In this paper, 11.5 kHz has been selected as the resonant frequency as well as the switching frequency of the system (parameters given in Table 1) to maintain the efficiency of 69.68% for an air gap of 16 cm, misalignment of 3 cm and load resistance of 36.6 Ω. For switching frequency control (on-off control) of the inverter, a state controller has been used.

Table 1. Simulation parameters and component values

Parameter	**Value**	**Parameter**	**Value**
Number of turns of transmitter coil	20	Load resistance, R_0	36.6 Ω
Number of turns of receiver coil	16	Switching frequency / resonant frequency	11.5 kHz / 11.5 kHz
Inner radius of transmitter and receiver coils	4 cm	C_{11}, C_{22} / L_{11}, L_{22} (Z-source network)	4.5 mF / 1 mH
Axial width of transmitter and receiver coils	16 cm	Leakage Inductance L_1 / L_2	152.6 μH / 97.64 μH
Conductor thickness	0.65 cm	Compensating capacitance C_1 / C_2	1.33 μF / 1.96 μF
Ferrite core dimension [cm]	42 × 42 × 0.45	Mutual inductance M	30.31 μH
Aluminum shield dimension [cm]	44 × 44 × 0.45	R_1 / R_2 (resonant circuit)	4 mΩ / 3.2 mΩ
Air gap	16 cm	Coupling coefficient	0.25
Lateral misalignment	3 cm		
AC input voltage, v_{ac} (phase value)	90 V RMS, 50 Hz		

An air gap and misalignment in a CPT system plays an important role in deciding the overall power transfer efficiency (PTE) of the system. Any change in an air gap and misalignment will affect the efficiency of the system considerably. In present study, a 16 cm air gap and 3 cm misalignment have been chosen to achieve the efficiency of the system around 70% for a resonant frequency of 11.5 kHz. Moreover, a 16 cm air gap and 3 cm lateral misalignment tolerance are sufficient for electric vehicle charging applications [3].

Values of compensating capacitors have been chosen as per the resonant frequency as given in Table 1. Selection of compensation topology is strongly related to application and selected power converter topology. In the proposed system, series-parallel (SP) compensation topology has been chosen as shown in Fig. 8. Series-parallel compensation means that one capacitor is connected in series to the transmitter coil and other one is connected in parallel to the receiver coil. Compared with other single-resonant CPT structures, the series-parallel (SP) compensation topology provides some useful advantages. The SP topology is the best choice for a battery charging system with a voltage source input as the current limitation is imposed by the parallel compensation in the secondary side [31, 32]. Moreover, series compensation is more effective to reduce the effects of leakage inductance in the primary side [33, 34].

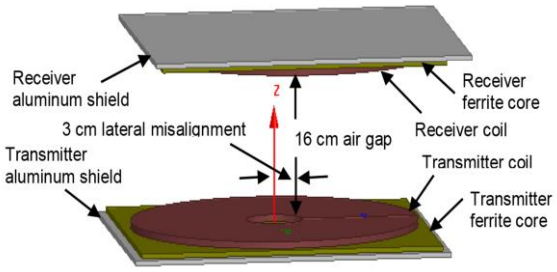

Fig. 5. Finite element model of the proposed CPT system

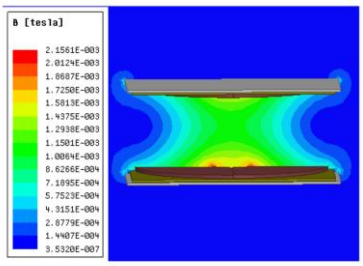

Fig. 6. Flux density distribution of the proposed CPT system

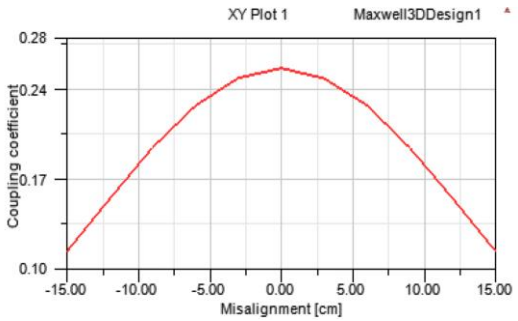

Fig. 7. Relationship between the coupling coefficient and lateral misalignment at an air gap of 16 cm

In Fig. 8, C_1 is the series compensating capacitor on the primary side and C_2 is the parallel compensating capacitor on the secondary side respectively. Circuit simulation results have been shown in Figs. 9-14 and 15 respectively. Fig. 9 shows the inverter output voltage (v_{inv}) and the primary-side resonant current (i_r) at full-load condition. It is observed in Fig. 9 that the primary-side resonant current flowing through the system is purely sinusoidal and in phase with primary-side voltage. Fig. 10 shows the secondary-side voltage and current. The primary side and secondary side voltage, current and power waveforms of the CPT transformer have been shown in Figs. 11 and 12 respectively.

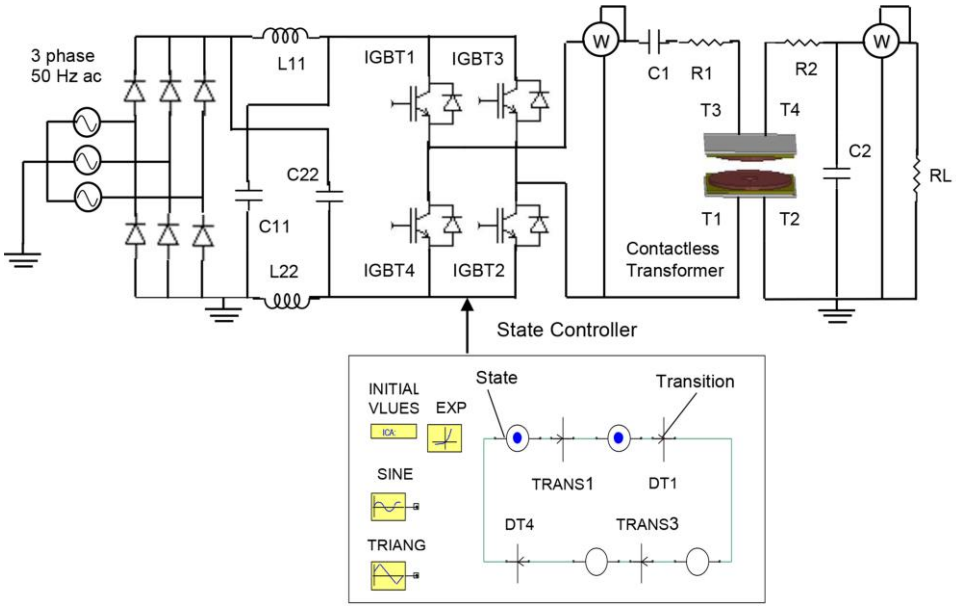

Fig. 8. Circuit simulation schematic with state controller

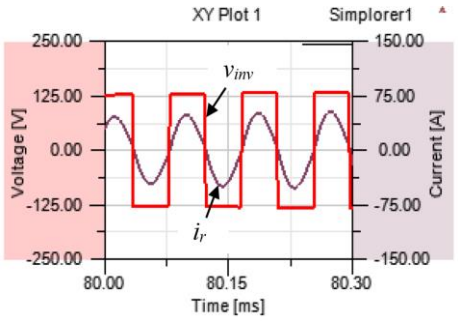

Fig. 9. Inverter output voltage and primary-side resonant current

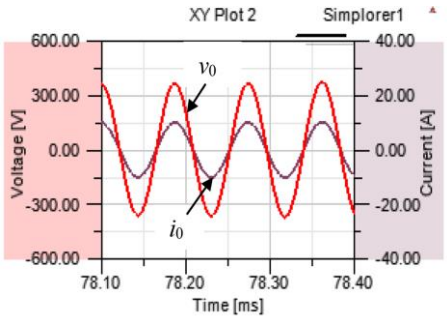

Fig. 10. Secondary side (output) voltage and current

In this analysis, the switching losses are considerable because the method used for output voltage regulation varies the active state duty cycle and this leads to hard switching. The input side rectifier conduction loss is also significant. The CPT system achieved an output power of 2 kW at a load resistance of 36.6 Ω for an input power of 2.87 kW. Based on the losses, from Figs. 11 and 12, it is observed that the proposed system has achieved an efficiency of 69.68% at full load condition. Figs. 13 and 14 show the Z-source capacitor and inductor voltages. It is observed that the Z-source capacitor and inductor voltages contain negligible ripples. In Fig. 15, primary and secondary power waveforms and average powers have been shown separately for the rated load. In Table 2, primary power, secondary power and efficiency of the system have been given.

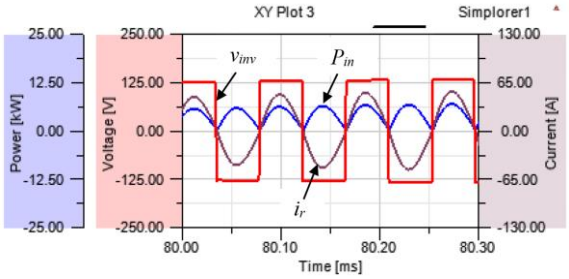

Fig. 11. Primary (input) voltage, current and power

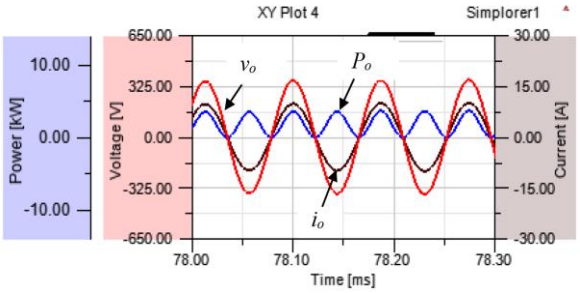

Fig. 12. Secondary (output) voltage, current and power

Table 2. Simulation results

Load resistance [Ω]	Primary power [kW]	Secondary power [kW]	Transformer efficiency [%]
36.5	2.87	2	69.68

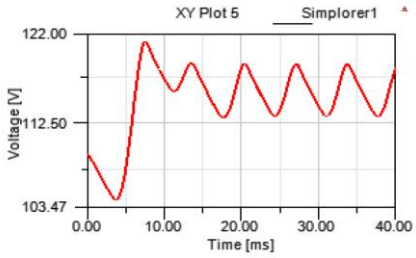

Fig. 13. Z-source capacitor voltage

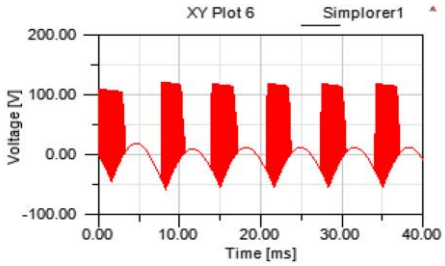

Fig. 14. Z-source inductor voltage

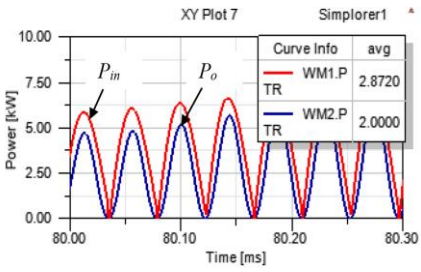

Fig. 15. Primary and secondary powers

4. Conclusions

In this paper, a new circuit topology for high power CPT applications using a full bridge Z-source resonant inverter has been developed and simulated. The Z-source network provides some unique features for the proposed system. The control methods in the system with the insertion of shoot-through modes of the Z-source inverter have been investigated. It has been observed from the results that the *dc* link voltage does not deviate with a wide range of load change, which is desirable for CPT systems. This is due to the Z-source network in the input side of the system. The Z-source network also makes the bridge inverter immune to the shoot-through states without any extra circuitry. In this study, a CPT system with a 16 cm air gap and 3 cm misalignment has been simulated. The present concept of design for CPT systems can be applied to low as well as high power applications. In the simulation, the proposed system attained an output power of 2 kW for a load resistance of 36.6 Ω. The overall system efficiency achieved is 69.68%. The low efficiency is due to the switching losses of the inverter and input-side rectifier conduction losses. From the waveforms, it is observed that the resonant current flowing in the system is purely sinusoidal and therefore no harmonics are injected into the source.

References

[1] Hui S.Y.R., Zhong W., Lee C.K., *A critical review of recent progress in mid-range wireless power transfer*, IEEE Transactions on Power Electronics, vol. 29, no. 9, pp. 4500-4511 (2014).

[2] Zhong W., Lee C.K, Hui S.Y.R, *General analysis on the use of tesla's resonators in domino forms for wireless power transfer*, IEEE Transactions on Industrial Electronics, vol. 60, no. 1, pp. 261-270 (2013).

[3] Huang Z., Wong S.C., Tse C.K., *Design methodology of a series-series inductive power transfer system for electric vehicle battery charger application*, IEEE Energy Conversion Congress and Exposition (ECCE), pp. 1778-1782 (2014).

[4] Tan P., Cao S., Gao X., *Adjustable coupler for inductive contactless power transfer system to improve lateral misalignment tolerance*, IEEE 8th International Power Electronics and Motion Control Conference (IPEMC-ECCE), pp. 2423-2426 (2016).

[5] Madawala U.K., Thrimawithana D.J., *A bidirectional inductive power interface for electric vehicles in V2G systems*, IEEE Transactions on Industrial Electronics, vol. 58, no. 10, pp. 4789-4796 (2011).

[6] Nguyen B.X., Vilathgamuwa D.M., Foo G.H.B. et al., *An efficiency optimization scheme for bidirectional inductive power transfer systems*, IEEE Transactions on Power Electronics, vol. 30, no. 11, pp. 6310-6319 (2015).

[7] Huang R., Zhang B., *Frequency, impedance characteristics and HF converters of two-coil and four-coil wireless power transfer*, IEEE Journal of Emerging and Selected Topics in Power Electronics, vol. 3, no. 1, pp. 177-183 (2015).

[8] Valtechev S., Borges B., Brandisky K., Klaassens J.B., *Resonant contactless energy transfer with improved efficiency*, IEEE Transactions on Power Electronics, vol. 24, no. 3, pp. 685-699 (2009).

[9] Feng H., Cai T., Duan S. et al., *An LCC-compensated resonant converter optimized for robust reaction to large coupling variation in dynamic wireless power transfer*, IEEE Transactions on Industrial Electronics, vol. 63, no. 10, pp. 6591-6601 (2016).

[10] McDonough M., *Integration of inductively coupled power transfer and hybrid energy storage system: a multiport power electronics interface for battery-powered electric vehicles*, IEEE Transactions on Power Electronics, vol. 30, no. 11, pp. 6423-6433 (2015).

[11] Li H., Li J., Wang K., Chen W., Yang X., *A maximum efficiency point tracking control scheme for wireless power transfer systems using magnetic resonant coupling*, IEEE Transactions on Power Electronics, vol. 30, no. 7, pp. 3998-4008 (2015).

[12] Zhang W., Mi C.C., *Compensation topologies of high-power wireless power transfer systems*, IEEE Transactions on Vehicular Technology, vol. 65, no. 6, pp. 4768-4778 (2016).
[13] Van S.K., Puers R., *Inductive powering, basic theory and application to biomedical systems*, Springer Science (2009).
[14] Monti G., Arcuti P., Tarricone L., *Resonant inductive link for remote powering of pacemakers*, IEEE Transactions on Microwave Theory and Techniques, vol. 63, no. 11, pp. 3814-3822 (2015).
[15] Li X., Tsui C.Y., Ki W.H., *A 13.56 MHz wireless power transfer system with reconfigurable resonant regulating rectifier and wireless power control for implantable medical devices*, IEEE Journal of Solid-State Circuits, vol. 50, no. 4, pp. 978-989 (2015).
[16] Musavi F., Eberle W., *Overview of wireless power transfer technologies for electric vehicle battery charging*, IET Power Electronics, vol. 7, no. 1, pp. 60-66 (2014).
[17] Peng F.Z., *Z-source inverter*, IEEE Transactions on Industry Applications, vol. 39, no. 2, pp. 504-510 (2003).
[18] Ellabban O., Abu-Rub H., *Z-source inverter: topology improvements review*, IEEE Industrial Electronics Magazine, vol. 10, no. 1, pp. 6-24 (2016).
[19] Huang L., Hu A.P., Swain A.K., Su Y., *Z-impedance compensation for wireless power transfer based on electric field*, IEEE Transactions on Power Electronics, vol. 31, no. 11, pp. 7556-7563 (2016).
[20] Zeng H., Peng F.Z., *High power factor Z-source resonant wireless charger*, IEEE Applied Power Electronics Conference and Exposition (APEC), pp. 1430-1434 (2017).
[21] Wang T., Liu X., Tang H., Ali M., *Modification of the wireless power transfer system with Z-source inverter*, IEEE Electronics Letters, vol. 53, no. 2, pp. 106-108 (2017).
[22] Zeng H., Peng F.Z., *SiC-based Z-source resonant converter with constant frequency and load regulation for EV wireless charger*, IEEE Transactions on Power Electronics, vol. 32, no. 11, pp. 8813-8822 (2017).
[23] Tianfeng W., Xin L., Houjun T. et al., *Modeling and advanced control of wireless power transfer system with Z-source inverter*, IEEE 2nd Annual Southern Power Electronics Conference (SPEC), pp. 1-6 (2016).
[24] Ellabban O., Mierlo J.V., Lataire P., *A DSP-based dual-loop peak dc-link voltage control strategy of the z-source inverter*, IEEE Transactions on Power Electronics, vol. 27, no. 9, pp. 4088-4097 (2012).
[25] Babaei E., Asl E.S., *High voltage gain half-bridge z-source inverter with low-voltage stress on capacitors*, IEEE Transactions on Industrial Electronics, vol. 64, no. 1, pp. 191-197 (2017).
[26] Zeng H., Yang S., Peng F.Z., *Wireless power transfer via harmonic current for electric vehicles application*, IEEE Applied Power Electronics Conference and Exposition (APEC), pp. 592-596 (2015).
[27] Huh J., Lee S.W., Lee W.Y. et al., *Narrow-width inductive power transfer system for online electrical vehicles*, IEEE Transactions on Power Electronics, vol. 26, no. 12, pp. 3666-3679 (2011).
[28] Keeling N.A., Covic G.A., Boys J.T., *A unity-power-factor IPT pickup for high-power applications*, IEEE Transactions on Industrial Electronics, vol. 57, no. 2, pp. 744-751 (2010).
[29] Park C.B., Lee H.W., *Study on the optimal switching frequency for maximum wireless power transfer in a variable airgap system*, IEEE Journal of Emerging and Selected Topics in Power Electronics, vol. 3, no. 1, pp. 201-204 (2015).
[30] Yu J., Hasko D.G., Nathan A., *Frequency selection for high efficiency wireless power transfer*, Journal of Display Technology, vol. 12, no. 7, pp. 681-684 (2016).
[31] Chao Y.H., Shieh J.J., Pan C.T., Shen W.C., *A closed-form oriented compensator analysis for series-parallel loosely coupled inductive power transfer systems*, IEEE Power Electronics Specialists Conference (PESC), pp. 1215-1220 (2007).
[32] Zhang W., Wong S.C., Tse C.K., Chen Q., *Load-independent duality of current and voltage outputs of a series- or parallel-compensated inductive power transfer converter with optimized efficiency*, IEEE Journal of Emerging and Selected Topics in Power Electronics, vol. 3, no. 1, pp. 137-146 (2015).
[33] Zhou W., Ma H., *Design Considerations of compensation topologies in ICPT system*, 22nd Annual IEEE Applied Power Electronics Conference and Exposition (APEC), pp. 985-990 (2007).
[34] Zhang W., Wong S.C., Tse C.K., Chen Q., *Design for efficiency optimization and voltage controllability of series–series compensated inductive power transfer systems*, IEEE Transactions on Power Electronics, vol. 29, no. 1, pp. 191-200 (2014).